



A Neural network-based Super Capacitor of a Multimachine Power System connected with a Renewable Energy sources

M. Bindu Priya

Assistant Professor, Department of EECE, GITAM (deemed to be university), Hyderabad, India

Email: bmadhu@gitam.edu

Dr. U. Salma

Associate Professor, Department of EECE, GITAM (deemed to be university), Visakhapatnam, India

Email: summe@gitam.edu

ARTICLE INFO

Received: 20 Sep 2024

Accepted: 25 Oct 2024

ABSTRACT

The paper advocates for the adoption of DC transmission based on voltage source converters (VSCs) as the future of offshore power transmission. It focuses on connecting onshore grids with offshore wind farms through innovative system design. The wave of the future for offshore power transmission is DC transmission based on voltage source converters (VSCs). Connecting onshore grids with offshore wind farms is the primary goal of this paper's DC transmission system design. Using DC at the grid side converter in tandem with a squirrel cage induction machine forms a large-capacity, low-speed flywheel energy storage system (FESS), as described in this article. Instead of being wasted as resistive losses, the FESS is specifically designed to absorb surge power, which occurs because of power flow imbalances during faults. It has been shown that the flywheel may successfully alleviate this issue due to the short length of these surges. The FESS is utilized for power evening out usefulness during ordinary activity and for fault ride-through assistance during fault circumstances. Illustrate the integration of offshore wind farms with onshore grids using DC transmission based on VSCs, highlighting the significance of this approach. Showcase the flow of power within the system, emphasizing the utilization of FESS to mitigate power flow imbalances during faults and maintain stability.

Keywords—Faults, Active and reactive power Loss, AC voltage control, VSC HVDC, offshore wind energy, PID, NN, THD.

Introduction

There have been major effects on productivity and daily living due to the energy crisis recently. The benefits of offshore winds outweigh those of onshore winds, which generate more electricity. The current favourite for far offshore wind applications is DC transmission architecture, because to its greater power and long-distance transmission capabilities. For offshore wind farm projects, several articles have contrasted HVAC and HVDC transmission technologies. Reference [1] shown that HVDC is superior to HVAC in terms of fault recovery capabilities. While HVAC is more cost-effective for power facilities under 300 MW, HVDC is the savviest choice for transmission systems that span greater distances [2].

According to research on system loss, HVAC systems are 12% more expensive than HVDC systems for big power plants and long distances [3]. Therefore, conventional HVAC transmission across long distances and huge power wind farms face serious challenges, such as increased costs and device losses during maintenance. A new transmission architecture using an ac cable and an onshore converter was described in reference [4]. The capacity of the receiving-end grid and the size of the dc grid are its limitations. The rapid growth of offshore wind resources at shorter distances has shifted the focus to wind farms capable of producing more electricity over longer distances. Of paramount importance for offshore wind farms, therefore, is the HVDC transmission

infrastructure. Two common converters are VSC and LCC. For offshore converters, LCC isn't an option for island operations, and for onshore converters, it means frequent commutation failures. When compared to VSC-HVDC, LCC-HVDC is not flexible enough to be used in real-world offshore wind farm projects. There is a wealth of literature outlining the various control and operating techniques used in real-world VSC-HVDC applications. Offshore wind farms use VSC-HVDC, however there is little research on the topic. Therefore, several VSC-HVDC topologies, operating techniques, and fault through mechanisms will be reviewed in this study. In an AC system, the generation of electric and magnetic fields results in a subtle but noticeable change in background energy flow, which engineers call reactive power. During an AC cycle, the stored energy in these fields varies. Reactive power is absorbed by devices like transformers and reactors that store energy by means of electric fields, and generated by devices like capacitors that store energy by means of magnetic fields created by current flows. A power system can only function within safe voltage ranges when actual and prospective power flows are tightly regulated.

A 'zonal foundation' for reactive power balances between generating sources and demand sites is required because reactive power flows may cause large voltage fluctuations across the system. A system's voltages, in contrast to its frequency, which remains constant across all nodes in the network, take the shape of a "voltage profile" that is dependent on current demand and generation in each node as well as the current configuration of the network. There is a 50/60 Hz alternating current and voltage, which does not always occur simultaneously. There is a vibrating quality to these amounts. As a result, the electricity "pulsates" as it travels down a single line, but at a rate of 100 times per second instead of 50. Both reactive and actual power are supplied and used by the various components of AC systems. Using actual electricity allows us to do practical tasks, such as running motors and lighting lights. Reliability of the system depends on the voltages that must be managed, and reactive power provides that support. In alternating current power networks, reactive power is used to adjust voltage magnitudes for system dependability, voltage stability, and operational acceptability. Active power is used to represent useful work.

Voltage Stability

For a power system to function within acceptable voltage limits, it is necessary to meticulously regulate power flows, whether real or potential. Real power delivery to consumers may be significantly enhanced with the help of reactive power, which is also essential for the dependable operation of the gearbox system. To get around transmission limitations and get cheaper actual power, it is occasionally possible to increase reactive power output at certain places (often close to a load centre). Proper operation of electric power equipment, preservation of equipment from impending damage, reduction of transmission losses, preservation of system resilience to disturbances, and prevention of voltage collapse all depend on voltage control, which entails keeping voltage within specified limits in an electric power system.

Commonly, under-voltages might be caused by:

- Supply transformers becoming overloaded
- The supply point has an inadequate short circuit level
- Significant voltage loss due to a lengthy feeder
- The linked load's low power factor
- Problems with remote systems that are being resolved
- The time it takes for an auto-reclose to close again
- The launch of high-powered induction motors.

Voltage Collapse

A voltage collapse phenomenon occurs when voltages in a certain region drop dangerously low or when a blackout happens as a result of the domino effect of voltage instability. In most cases, voltage collapse occurs when a power system is either overloaded or lacks insufficient reactive power to sustain the load.

Table 1: DC transmission topologies comparison

Topology	<i>advantages</i>	<i>disadvantages</i>
<i>Point-to-point [5]</i>	1.Simplified protection configuration; 2.engineering application.	1.More dc cables and sea area.
<i>Radial [3]</i>	1.save resource of dc cables and sea area; 2.engineering application.	1.large occupation area and high cost of offshore converter ; 2.interacts with each WF.
<i>Radial+[5]</i>	1. save resource of dc cables and sea area.	1.DC breaker configuration.
<i>Wind farm ring [6]</i>	1. offshore transmission flexibility.	1.dc breaker configuration 2.complicated protection configuration; 3. large occupation area and high cost of offshore converter.
<i>Substation ring [6]</i>	1. receiving-end grid flexibility.	1.dc breaker configuration; 2.complicated protection configuration.

VSC HVDC Transmission System

It is possible to change the voltage of electrical power from AC to HVDC or vice versa using an HVDC converter. For long-distance electrical transmission or interconnection between AC power systems operating at various frequencies, HVDC is a viable alternative to AC. It is theoretically possible to construct HVDC converters with even greater ratings; those with a capacity to convert two gigawatts (GW) and a voltage rating of up to 900 kilovolts (kV) already exist. A full converter station could include many of these converters connected in parallel or series. The most common and preferred method of transmitting electricity across long distances or underwater is using high voltage DC transmission lines, which use direct current (DC). These typically have two converter terminals linked by a DC transmission line, although multi-terminal HVDC with interconnected DC transmission lines are also used in some situations. Types of High-Voltage Direct Current (HVDC) systems include Back-to-Back DC and HVDC Light. Compared to conventional HVDC, HVDC Light is more cost-effective at lower power levels because to its use of modern cable and converter technology. The conventional method seeks to avoid dissipating this surplus energy by use of a chopper circuit that is linked in parallel with the DC connection and then passed via a resistor. This research proposes a FESS that, rather of wasting the excess energy, may store it as a power differential. Meanwhile, HVDC devices are able to keep their voltage levels stable. Conversely, the FESS is utilized for wind power evening out during customary activity, which is necessary since wind energy is intermittent. The most catastrophic AC side fault that may lead to power going out entirely is a three-phase-to-ground short circuit. The energy should have been put away during a shortcoming, which is subject to the requirements for issue ride through, may inform the design of the FESS converter. The FESS converter has to have a similar rating as the breeze ranch for it to store the wind farm's rated power in the event of an AC failure. As seen in figure 1, the powerful flywheel is pushed by an acceptance machine, which is a suitable choice for power conditioning applications owing to its resilience in the face of extreme operating mode changes.

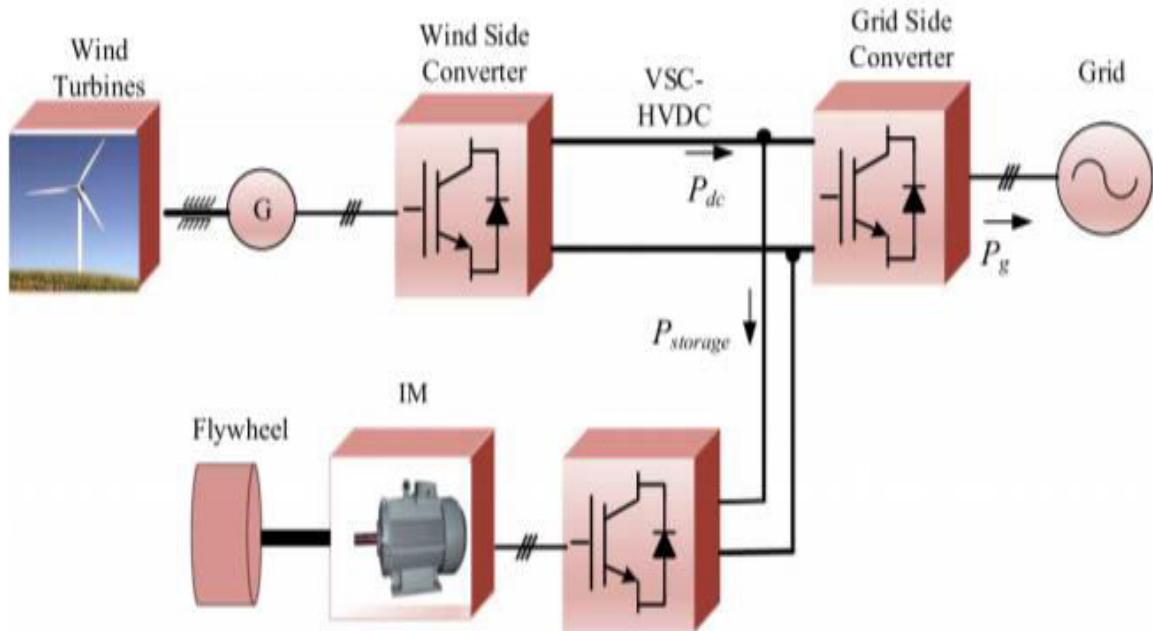


Figure 1: Shows a VSC-HVDC gearbox system integrated with FESS.

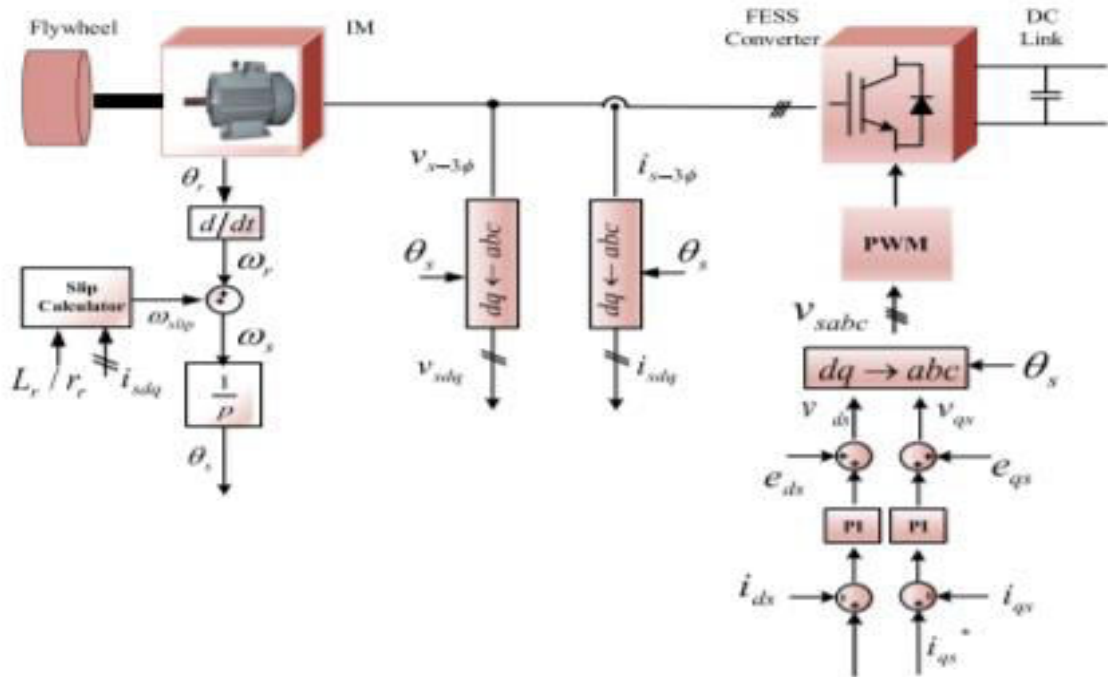


Figure 2: A schematic depicting the suggested FESS control technique that is grounded in IFOC

Induction Machine and FESS Converter Modeling:As seen in figure 2, the primary objective of the recommended control procedure is to direct the FESS in both normal and fault situations. The traditional indirect field-oriented control (IFOC) system provides the basis for controlling the enlistment machine that controls the flywheel. By monitoring the machine's voltages and currents, we can measure the quick FESS stator dynamic power. This value is then contrasted with the power differential between the grid and wind. A power regulator with many controllers works to correct power errors. This work presents in-depth simulation findings with the development and description of a model for an enlistment machine-controlled flywheel capacity framework. The model has been built in MATLAB/Simulink after a thorough examination of the IM's loss. Further, the machine's operation is examined in terms of driving and generating modes that regulate the flywheel storage's charge-discharge cycles. The FESS is a device that uses kinetic storage, which involves a spinning mass that can hold its inactivity, to store energy. There are three modes that a flywheel storage system

may operate in: acceleration, standby, and deceleration. Among the many components that make up FESS are its bearing system, power electronics, engine/generator set, flywheel rotor, and low-pressure vacuum control. Taken as a whole, these parts define the FESS's total efficiency.

Flywheel Rotor: A rotating mass m (kg) with inertia J (kg·m²), spinning at an angular velocity of $\dot{\omega}$ (rad/s), stores kinetic energy E (joules) according to Equation, and is used as the rotor of the flywheel.

$$E = \frac{1}{2}J\omega^2$$

If a flywheel is spun between two points with a base and greatest speed of $\dot{\omega}$, its usable stored kinetic energy may be expressed as

$$E = \frac{1}{2}J(\omega_{max}^2 - \omega_{min}^2)$$

situated at the instant of static equilibrium Variables such as flywheel mass and shape determine J . Here is an equation that may be used to represent the angular velocity of a circle type flywheel: m kg, ρ kg/m³, and l m.

$$\omega = \frac{2}{r} \sqrt{\frac{E}{\rho\pi l}}$$

Based on this, Equation represents the stored energy.

$$E = \frac{1}{4}mr^2(\omega_{max}^2 - \omega_{min}^2)$$

If we consider a round and hollow flywheel with internal and external radii r_1 and r_2 , we can get the stored kinetic energy using Equation.

$$E = \frac{1}{4}m(\omega_{max}^2 - \omega_{min}^2)(r_2^2 - r_1^2)$$

Different types of electrical losses, such as those experienced by the power converter, stator, and rotor, all have an impact on the conversion efficiency of a FESS. The bearing misfortunes and the streamlined or windage misfortunes are the primary causes of the system's mechanical losses. The equilibrium of power Equation is the formula for the squirrel confine enlistment machine FESS (SCIM-FESS).

$$P_{out} = P_{ag} - P_{rcl} - P_{rfe} - P_{mech}$$

$$P_{ag} = P_{in} - P_{scl} - P_{sfe}$$

$$P_{out} = P_{in} - P_{scl} - P_{rcl} - P_{rfe} - P_{sfe} - P_{mech}$$

$$P_{in} = P_{out} + P_{scl} + P_{rcl} + P_{rfe} + P_{sfe} + P_{bearing} + P_{windage}$$

The following variables are defined in this context: P_{ag} , the power transferred from the stator to the rotor of an IM across the air gap; P_{in} , the input power; P_{out} , the total output power; P_{scl} , the stator copper loss of the IM; P_{rcl} , the rotor copper loss of the IM; P_{rfe} , the core loss in the stator; P_{sfe} , the rotor core loss; $P_{bearing}$, the bearing loss of the FESS; and $P_{windage}$, the gearbox loss of the FESS When operating within a specific speed range, critical parameters that must be managed in a FESS include the DC-link voltage (V_{dc}), electromagnetic torque (T_e), speed ($\dot{\omega}_m$), and the location of the rotor magnetic flux vector (θ_e). In order to regulate the gate pulses, field oriented control (FOC) and space vector pulse width modulation (SVPWM) have been used. The FOC has a straightforward control structure similar to a DC machine, with reduced parameter variation uncertainty, since it regulates the torque generating current (i_q) and the magnetic flux producing current (i_d) independently. Measuring the currents in the three phases of the stator creates the feedback loop, which is then turned into the coordinated d-q reference utilizing Park's change. To produce door beats for the main side converter using an SVPWM modulator, the DC stator flows i_{ds} and i_{qs} are contrasted and reference flows i_{ds}^* and i_{qs}^* utilizing PI current controllers. The flux estimator compares the reference flux with the actual magnitude of the rotor magnetic flux, is calculated. The reference d-q axis currents, denoted as (i_{ds}^* and i_{qs}^*) are determined by the currents (i_d) and (i_q) calculator blocks, respectively. The reference voltages (V_{dref} and V_{qref}) are the result of comparing the actual stator currents with the determined reference upsides of the flows in the simultaneous d-q reference outline. Essential to this kind of control is the rotor flux angle, which, when applied to an induction motor, establishes the location of the rotor flux.

$$\lambda^{est} = \frac{L_m i_d}{1 + sT_r}$$

$$i_{ds}^* = \frac{\lambda_d}{L_m} \quad i_{qs}^* = \frac{2}{3} \cdot \frac{2}{P} \cdot \frac{L_r}{L_m} \cdot \frac{T_e^*}{\lambda^{est}}$$

$$\theta_e = \int (\omega_m + \omega_{sl})dt \quad \omega_{sl} = \frac{i_{qs}^*}{i_{ds}^*} \cdot \frac{1}{T_r}$$

The following variables are used in the equation: λ_{est} stands for an estimated flux, λ_d for the d-axis rotor magnetic flux linkage, T_e^* for the reference electromagnetic force created by the PI regulator, L_m and L_r for the shared inductance and rotor inductance, ω_{sl} for the slip frequency, T_r for the rotor time constant, i_{ds}^* and i_{qs}^* for the reference stator currents, and so on.

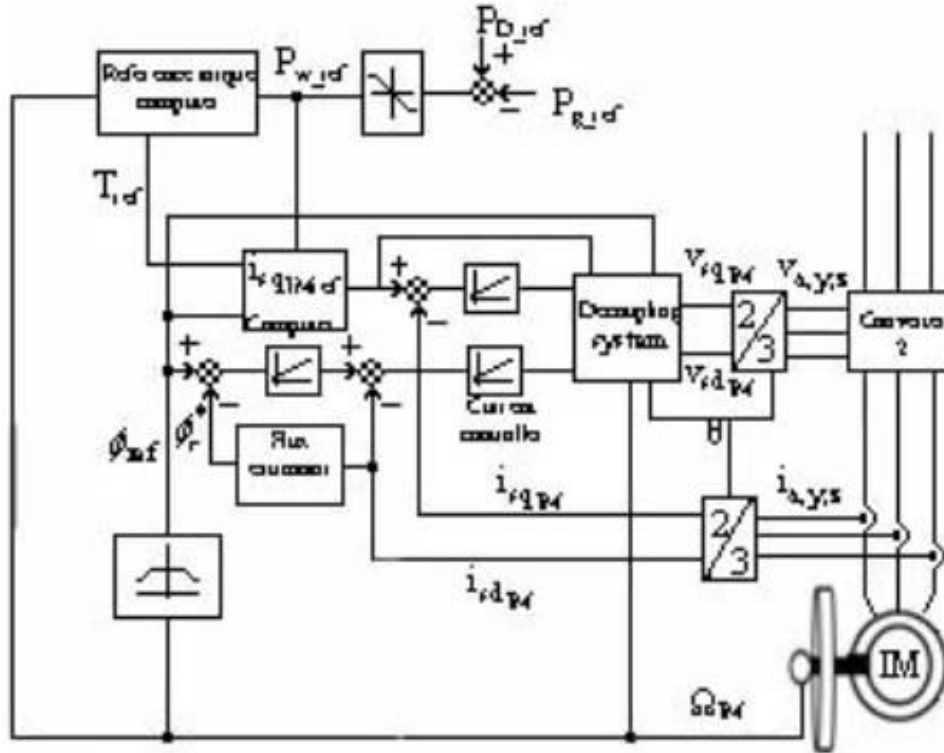


Figure 3: FESS Induction machine control scheme

The research demonstrates that the IM-FESS has desirable properties in terms of energy control and dynamic reactivity in light of changes in load torque. The vector control approach is used by the IM drive system to direct the power electronics converters to obey the torque, speed, and voltage reference value instructions. In less than 5 milliseconds, the IM transitions from generator mode to engine mode, and the machine-side field-situated control framework swiftly reverses the magnetic field in response to the reversal of torque. In data centre applications, for example, where critical loads need rapid response, this might be advantageous. In order to increase stability at the connection point while integrating the flywheel with sustainable sources in an electric matrix, the vector regulator of the framework converter keeps the DC voltage constant under diverse load situations. Using an IM-FESS in a power grid that incorporates a wind energy system is the primary goal of future studies with this model.

Mathematical Steady Model of VSC-HVDC System:

It is recommended to use the same per-unit esteem framework for both the air conditioner and DC systems for simulating and calculating hybrid power systems. The following is an introduction to the per-unit value system provided in this paper [7]:

$$P_{dB} = S_B, \dots\dots\dots(1)$$

$$U_{dB} = U_B, \dots\dots\dots(2)$$

$$I_{dB} = \sqrt{3}I_B, \dots\dots\dots(3)$$

$$R_{dB} = Z_B, \dots\dots\dots(4)$$

In this case the reference power of the AC system is S_B and the DC system is P_{dB} . In the air conditioner side of the converter, the reference voltage U_B , reference current I_B , and reference impedance Z_B are the following values: On the DC side of the converter, the reference voltage U_{dB} , reference current I_{dB} , and reference impedance Z_{dB} are

the proper values. One VSC station acts as a rectifier and the other as an inverter; these two stations are essential components of the VSC-HVDC system. Connection types between VSC stations and VSC-HVDC may range from two-terminal to multi-infeed DC systems, depending on the specific application [1-3]. The actual model for a multi-terminal DC framework with VSC-HVDC is shown graphically in figure. 3, which shows the steady state. This is the per-unit system (p.u.) that the VSC-HVDC stable models are presented in.

$$\mathbf{I}_i = \frac{\mathbf{U}_{si} - \mathbf{U}_{ci}}{R_i + jX_{li}}, \dots\dots\dots(5)$$

$$\widetilde{S}_{si} = P_{si} + jQ_{si} = \mathbf{U}_{si}\mathbf{I}_i^*, \dots\dots\dots(6)$$

$$P_{si} = -|Y_i|U_{si}U_{ci} \cos (\delta_i + \alpha_i) + |Y_i|U_{si}^2 \cos \alpha_i, \dots\dots\dots(7)$$

$$Q_{si} = -|Y_i|U_{si}U_{ci} \sin (\delta_i + \alpha_i) + |Y_i|U_{si}^2 \sin \alpha_i + \frac{U_{si}^2}{X_{fi}}, \dots\dots\dots(8)$$

$$P_{ci} = |Y_i|U_{si}U_{ci} \cos (\delta_i - \alpha_i) - |Y_i|U_{ci}^2 \cos \alpha_i, \dots\dots\dots(9)$$

$$Q_{ci} = -|Y_i|U_{si}U_{ci} \sin (\delta_i - \alpha_i) - |Y_i|U_{ci}^2 \sin \alpha_i, \dots\dots\dots(10)$$

$$P_{di} = U_{di}I_{di} = |Y_i|U_{si}U_{ci} \cos (\delta_i - \alpha_i) - |Y_i|U_{ci}^2 \cos \alpha_i, \dots\dots\dots(11)$$

$$U_{ci} = \frac{\sqrt{6}M_iU_{di}}{4}. \dots\dots\dots(12)$$

All of the variables used in the equations (5) through (12) are [14].

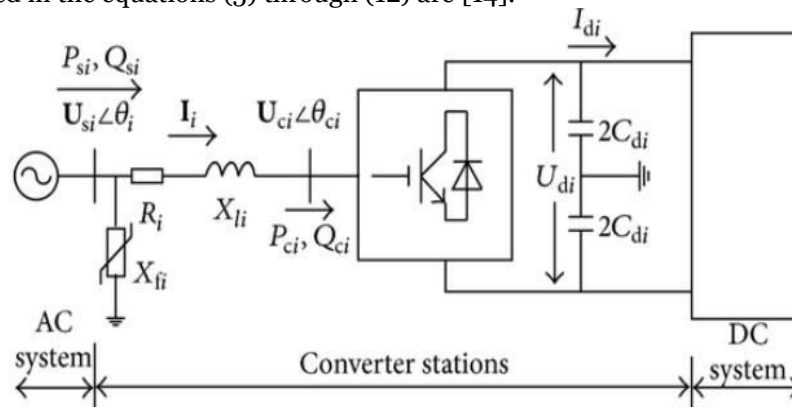


Figure 4: Schematic of the multi-terminal VSC-HVDC physical model in steady state.

Steady-State Control Modes of VSC-HVDC: Due to the presence of fully adjustable power electronic switch semiconductors such entryway switches off thyristors and protected door bipolar semiconductors, VSC-HVDC can independently regulate reactive and active power at its terminals. As a result, a few of commonly used control objectives may be established for every VSC as shown in figure 4.

1. Active power control for the AC system establishes the amount of active power transferred.
2. The purpose of DC voltage regulation is to maintain a consistent DC voltage.
3. The measure of receptive power that is traded with the air conditioner framework is controlled by AC reactive power.
4. Direct control of alternating current voltage, as a measure for the system bus voltage, as an alternative to reactive power regulation.

The following four groups comprise the majority of VSC control methods:

- Constant DC voltage control, constant AC reactive power control
- Constant DC voltage control, constant AC voltage control
- Constant AC active power control, constant AC reactive power control
- Constant AC active power control, constant AC voltage control

Pulse Width Modulation(PWM): As each network connected to its own power generation station, a converter linkage the two networks so that electric power may be sent from one to the other. On the Air conditioner side of the converter, there is a bridge of semiconductor switches that can turn off their gates. This bridge is connected to a control system, and it produces a bridge voltage waveform with a fundamental Fourier component at the frequency of the electric network associated with the air conditioner side of the converter. The three reference signal inputs in the control system enable the operator to adjust the basic Fourier component's frequency, amplitude, and phase angle, as well as the network's alternating voltage associated with the DC side of the converter via the control system [4].One distinguishing feature of VCS-HVDC gearbox is its capacity to control the receptive and genuine power stream at the Point of Common Coupling (PCC) separately for each AC system it is coupled to. Although the direction of power flow is switched from continuous to line commutated HVDC transmission, the DC interface voltage's extremity is kept up with by simply reversing the DC current.

Methods

PID controller:One kind of controller that finds frequent use in industrial settings is the proportional-integral-derivative conventional controller, also known as a closed-loop controller with negative feedback. In order to evaluate the potential error associated with the common value change, a controller with PID parameters must compare the measured processed variable to the intended set point on a frequent basis. Reducing the change in error over a certain time period is the primary goal of a controller, which is achieved by adjusting control variables. The Ziegler-Nicolas method, which is used by the PID controller, takes into account the three parameters—the proportional, integral, and derivative values—one by one. Subordinate of the boundaries, which gauge the outcome accomplished on proportionate rate with the errors, which vacillates continually; gain boundary of the relative regulator, which assesses the got blunder; and essential boundaries, which gauge the outcome in view of the amount of the errors. In sum, the process may be altered via the control components by combining three gain actions.

This controller maintains control actions for the plant's intended needs via the "tuning" of parameters in the PID algorithm. The PID controller's output is responsible for the controller's improved responsiveness via error minimization; the controller overshoot percentage is determined by the oscillation degree and system set point. A very stable system may not get the best answer when using a PID controller technique. There are three parameters that may be controlled in the system applications. For unwanted outputs, the ideal PID gain setting is to set the control to a null value. Figure 5 shows that PID controllers, which are also called PD, PI, P, or I controllers, do not perform the control actions that are indicated. When adjusting the gain of a PI controller, it is usual practice to use the derivative, which is accurate for measuring noise but ignores the integral gain. This causes the system to fail in its control action, which is to achieve an output value that is in accordance with the reference value.

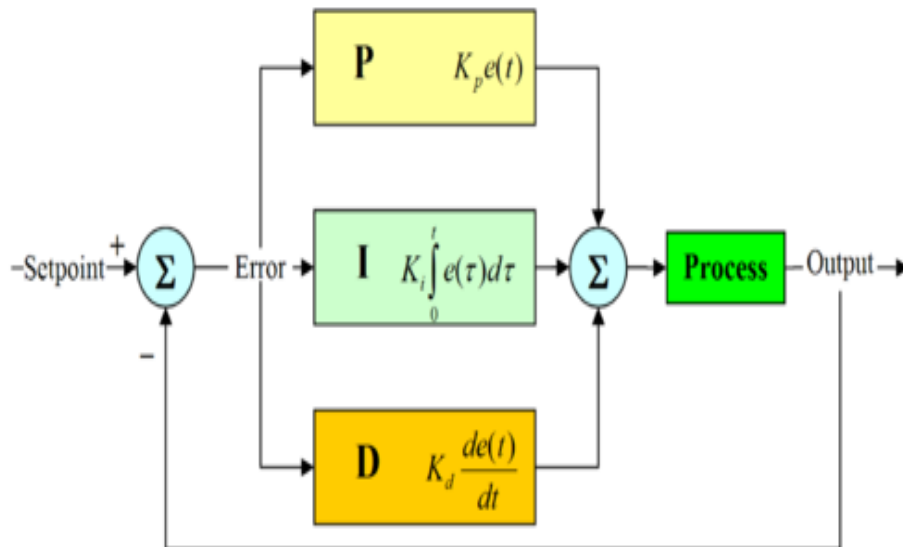


Figure5: PID controller block diagram representation

To assess the reaction of the PID regulator settings, the PID terms are obtained. The mathematical form of the controller output $u(t)$ may be obtained by:

$$u(t) = MV(t) = K_p e(t) + K_i \int_0^t e(\tau) d\tau + K_d \frac{de}{dt} \dots \dots \dots = (13)$$

1. K_p : Proportional gain – The reaction time is proportional to the size of K_p . System instability, as measured in oscillations, will be processed by a massive proportional gain.
2. K_i : Integral gain – The elimination of errors in steady state is indicated by a bigger K_i .
3. K_d : Derivative gain – A smaller percentage overrun, accompanied by instability and a delayed transient response, is achieved with a greater K_d .

Artificial Neural Network:

Simple components interact together in a parallel fashion to form neural networks. These components are based on the neural networks seen in living organisms. The interconnections between nodes in a network are essentially what dictate its operation, just as they are in the natural world. Training a neural network to carry out a task entails manipulating the values of the connections (weights) between its constituent parts. Typically, while training a Neural Network, its parameters are fine-tuned to ensure that a given input will produce the desired output. There, the network is fine-tuned by comparing the output to the goal and making adjustments until the two sets of data are in perfect alignment. Figure 6 shows an example of a network that has been trained using supervised learning with multiple input/target pairings.

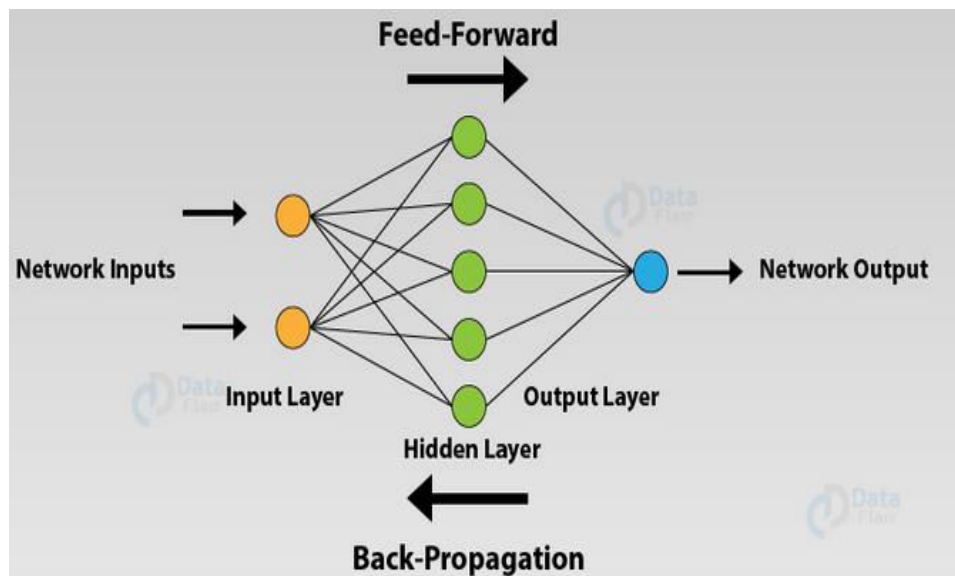


Figure6. Block diagram of Neural Network

In bunch preparing, an organization's loads and predispositions are adjusted using all of the input vectors in a single batch. With incremental training, a network's biases and weights are adjusted as required after the show of each info vector. One name for steady preparation is "adaptive" or "online" training. Design acknowledgment, ID, characterization, discourse, vision, and control frameworks are just a few of the many areas that have trained neural networks to execute complicated tasks. Nowadays, it is possible to train neural networks to tackle issues that are too complex for humans or traditional computers to handle:

Our goal is to identify and categorise five distinct types of HVDC transmission system failures. The primary procedures for fault classification on HVDC systems are as follows:

- Variables for input and output selection
- Handling inputs and outputs.
- Neuronal network architecture
- Fault-based pattern generation for use in training and testing
- Network-based training
- A test pattern evaluation for the classifier that has never been seen before

An essential building block of every neural network is the information processing unit known as a neuron. The building blocks of neural networks are shown in the block diagram of a neuron in Fig. 6. In this section, we outline the three fundamental components of the neural model.

- A network of synapses, or linkages, where each connection has its own unique strength.
- A neuron-specific adder that takes into account the relative strengths of the synapses to calculate the total input signal.
- An activation function that controls how much of a spike a neuron can send out.

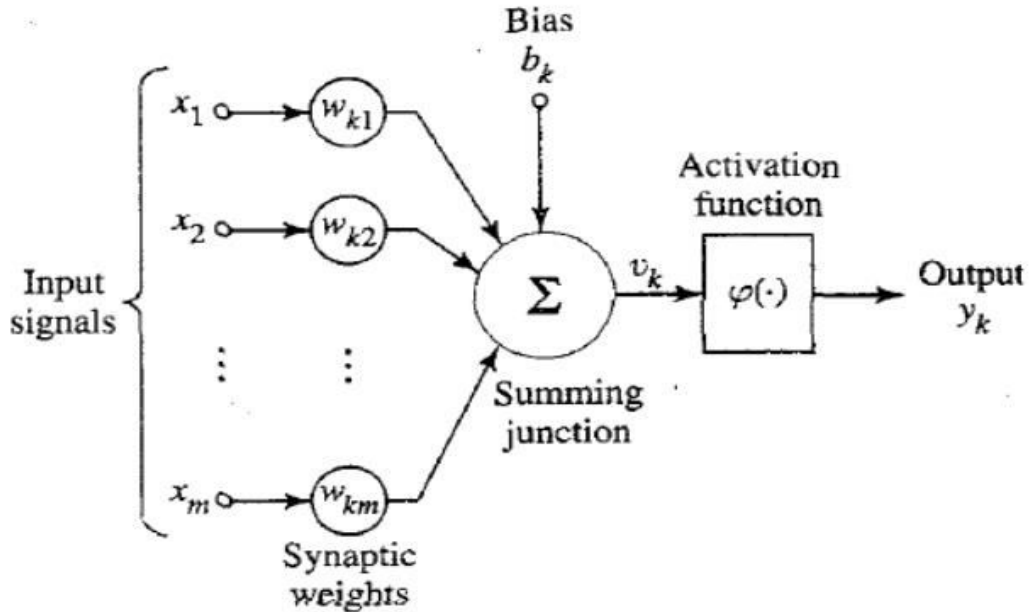


Figure 7: Nonlinear model of a neuron

Figure 6's neural model also incorporates a bias that is introduced from the outside, shown by b_k . As a function of its positive or negative value, the bias b_k raises or lowers the activation function's network input, accordingly.

$$u_k = \sum_{j=1}^m w_{kj} x_j \dots\dots\dots(14)$$

$$y_k = \varphi(u_k + b_k) \dots\dots\dots(15)$$

In where x_1, x_2, \dots, x_m denote the input signals, $w_{k1}, w_{k2}, \dots, w_{km}$ denote the synaptic weights of neuron k , u_k denotes the output of the direct combiner because of the info signals, b_k denotes the bias, φ , the activation function, and y_k is the neuron's output signal. In the model presented in Figure 7, the application of bias b_k applies an affine modification to the output u_k of the linear combiner, as shown by equations (16) and (17)

$$V_k = \sum_{j=0}^m w_{kj} x_j \dots\dots\dots(16)$$

$$y_k = \varphi(V_k) \dots\dots\dots(17)$$

An activation function takes all of the inputs into a neuron and uses them to determine the output power. The best activation function is selected based on the needs of the application. The primary challenge in developing ANNs is finding the appropriate weights to accomplish the goal. The terms "learning" and "training" often describe this procedure. In artificial neural network (ANN) learning, directed and solo learning are the two main approaches. The goal of supervised learning is to minimize the error, or the distinction between the info samples and the intended output values, by adjusting the network weights. This approach might be seen as a kind of "teaching" where the instructor is aware of the desired input-output relationships. A training vector is the set of input signals, and the intended response is the best course of action for the network to take. When the expected and actual network responses are different, this is called the error signal.

$$w_{ji}(n+1) = w_{ji}(n) + \Delta w_{ji}(n) \dots\dots\dots(18)$$

$W_{ji}(n)$ and $w_{ji}(n+1)$ stand for the weights that were previously what's more, amended between the i th and j th adjacent layers, respectively; $\Delta w_{ji}(n)$ is the value that was used for correction, and n is the quantity of emphasis steps. If the selection of corrections $\Delta w_{ji}(n)$ ensures that the computations from the previous iteration are convergent, then the learning process will be stable. Think about a single-layer network's j th neuron. Lessening the discrepancy between the j th neuron's actual output $y_j(n)$ and the value required by the instructor $d_j(n)$, as shown in equation, is the foundation of learning.

$$e_j(n) = d_j(n) - y_j(n) \dots\dots\dots(19)$$

Vector $e(n)$ stores all of these errors. The input weighting coefficients vector $w(n)$ to the layer under consideration determine the vector $e(n)$. The accompanying recipe might be utilized to determine the value of the adjustment in equation (18):

$$\Delta w_{jk}(n) = \eta e_j(n) x_k(n) \dots\dots\dots(20)$$

The i th input signal is represented by x_i , and the speed of the iteration process is determined by the learning rate parameter η . For learning to take place, the error function equation must be minimised (18,19). The error function for a network of L neurons may be expressed as in equation.(20):

$$S_2(w) = \frac{1}{2} \sum_{j=1}^L (d_j - y_j)^2 \dots\dots\dots(21)$$

If there are P learning pairings in the training set, where $x(n)$ is an input vector and $d(n)$ is a vector of intended outputs, then the error function for the n th iteration step of learning may be given by equation (21):

$$S_2(w(n)) = \frac{1}{2} \sum_{n=1}^P \sum_{j=1}^L (d_j(n) - y_j(n))^2 \dots\dots\dots(22)$$

The introduction of non-linear activation functions makes the minimization of equation (22) a non-linear issue. The good news is that the steepest-descent approach provides the basis for known efficient numerical methods that can minimise that function. The back-error-propagation learning approach relies on them as an analytical foundation. As a function of errors obtained from minimization of equation (22) the back-error-propagation method calculates correction values equation (21). Layer by layer, beginning at the output layer, the procedure is executed in the opposite manner throughout the network. Figure 8 showcases the algorithm's structure (7). Blocks $A(M), A(M-1), \dots, A(1)$ determine the corrected weighting vectors, whereas blocks $B(M-1), B(M-2), \dots, B(2)$ compute the mistakes that are "propagated" to the low layers. A wide variety of implementations of the back-error-propagation method are available. When mistakes are handed back starting with one layer then onto the next or after a specific iterative step is finalised, they may be effectively updated using several approaches for determining new weighting factors. By verifying the value of the corrections equation at consecutive phases, the network's "learning" grade may be assessed. The size of the network, their structure, the kind of the examined issue, the specifics of the learning algorithm, and other factors determine the quantity of iterative advances (equivalent to the size of the pre-arranged learning set) expected to get satisfactory assembly. There are instances when a learning set of several thousand cases is necessary.

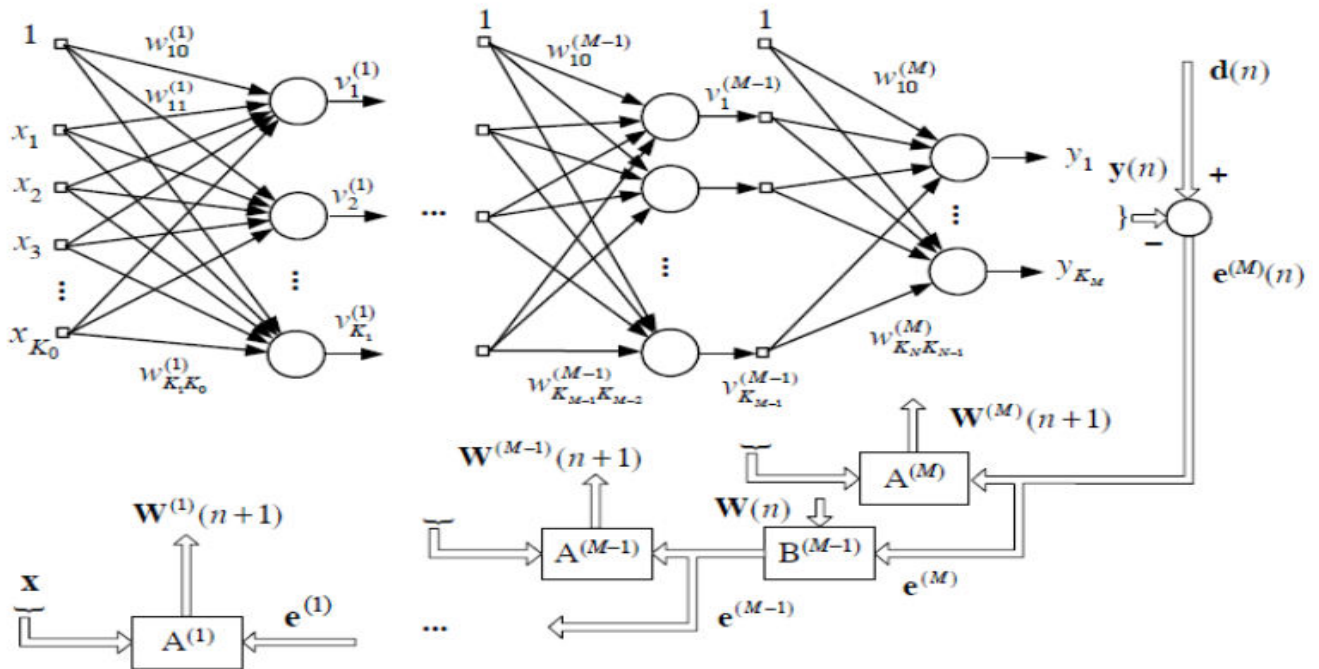


Figure8: Back-propagation Training network

Gathering an enormous number of models that grandstand every one of the numerous parts of the issue is the optimal training approach (more models are required for additional confounded issues). It is fairly uncommon to introduce noise or other forms of randomness into the preparation information to adjust the organization to the clamor and inherent unpredictability seen in real-world data. This helps to build a strong and trustworthy network. A network that is unstable and unpredictable is certain to result from using poor preparing information. It is normal practice to prepare the organization for a specific number of ages or until the result mistake falls under a specific edge.

- Choosing the Number of Neurons
- Choosing the Initial Weights

- Choosing the Learning Rate

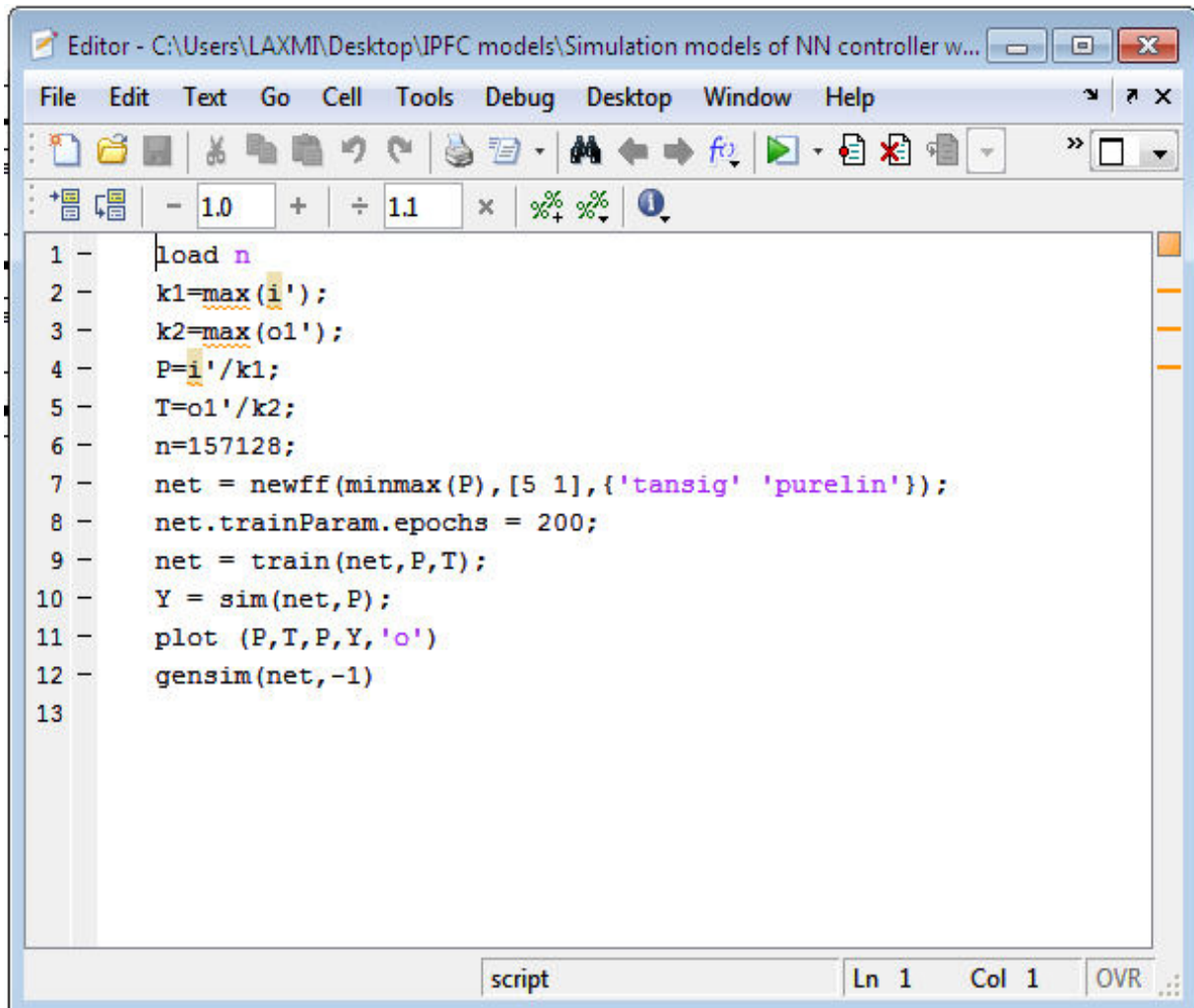
In most cases, `trainlm` is the quickest training function, and feed-forward net uses it by default. The selection of the power network was based on the following criteria:

- In order to reap the benefits, the network has to be operational in the real world.
- An HVDC network is required.
- A bipolar transmission line must be used.
- The length must be sufficient for detailed fault locating analysis.

Here, we detail the inquiry into fault analysis of HVDC systems using an artificial neural network (ANN). When it comes to iterative techniques that utilize the back propagation technique, neural networks are the quickest. With a big enough training set, the neural network can train quickly, has a built-in parallel structure, and will provide excellent classification results. In a typical neural network implementation, the quantity of sources of info, stowed away layers, and output layers is rather large. The neural network that was created for this study has one information layer, one result layer, and five secret layers of neurons that allow the system to compute more quickly. Data inputted into the neural network during training has been DC current. The rectifier's firing angle is the target, and the training process is back propagation. There are a number of AC inverter problems that may affect VSC HVDC systems, and the data on these faults has only ever been utilized for preparing and testing purposes. The neural network-based back-propagation method was trained using 25 data sets covering a range of VSC HVDC system operating conditions. Six data sets have been tested. The findings are shown after the neural network controller converged after 247 epochs of training the neural network system.

Discussion and Results

During typical operation, the wind farm must supply grid power of 0.6 pu, notwithstanding its fluctuating power profile. When the amount of wind power produced exceeds the demand from the grid, a FESS is used to provide energy storage. The FESS is then released when there is insufficient electricity from the wind turbine. The induction machine's quadrature-axis and direct-axis currents follow their reference values given by the PI and NN controllers, respectively. At 2 s, the grid converter controller receives a power reference of 1 pu, and the storage system's reference power is assumed to be zero. Step loading causes an abrupt increase in the DC link voltage. A three-stage to-ground disappointment happens at 4 seconds on the matrix side at Bus 1. Evaluating the system's resilience in the face of failure in both the energy storage medium- and fault-free-case scenarios. There is an abrupt cutoff of grid electricity to zero when a fault occurs. If the problem persists after 15 cycles, the capacity power reference is decreased to zero by and by. The drifters of the DC connect voltage are viewed as rather small. There is no change to the main inverter currents while the problem is occurring. Figures 9 to 22 show the outcomes of simulations for grid-connected variable speed controller (VSC) offshore wind farms that use flux injection (FID) and natural neural network (NN) controllers.



```
Editor - C:\Users\LAXMI\Desktop\IPFC models\Simulation models of NN controller w...
File Edit Text Go Cell Tools Debug Desktop Window Help
- 1.0 + ÷ 1.1 x % %
1 - load n
2 - k1=max(i');
3 - k2=max(o1');
4 - P=i'/k1;
5 - T=o1'/k2;
6 - n=157128;
7 - net = newff(minmax(P), [5 1], {'tansig' 'purelin'});
8 - net.trainParam.epochs = 200;
9 - net = train(net,P,T);
10 - Y = sim(net,P);
11 - plot (P,T,P,Y, 'o')
12 - gensim(net,-1)
13
script Ln 1 Col 1 OVR
```

Figure9: M-file program for NN Controller

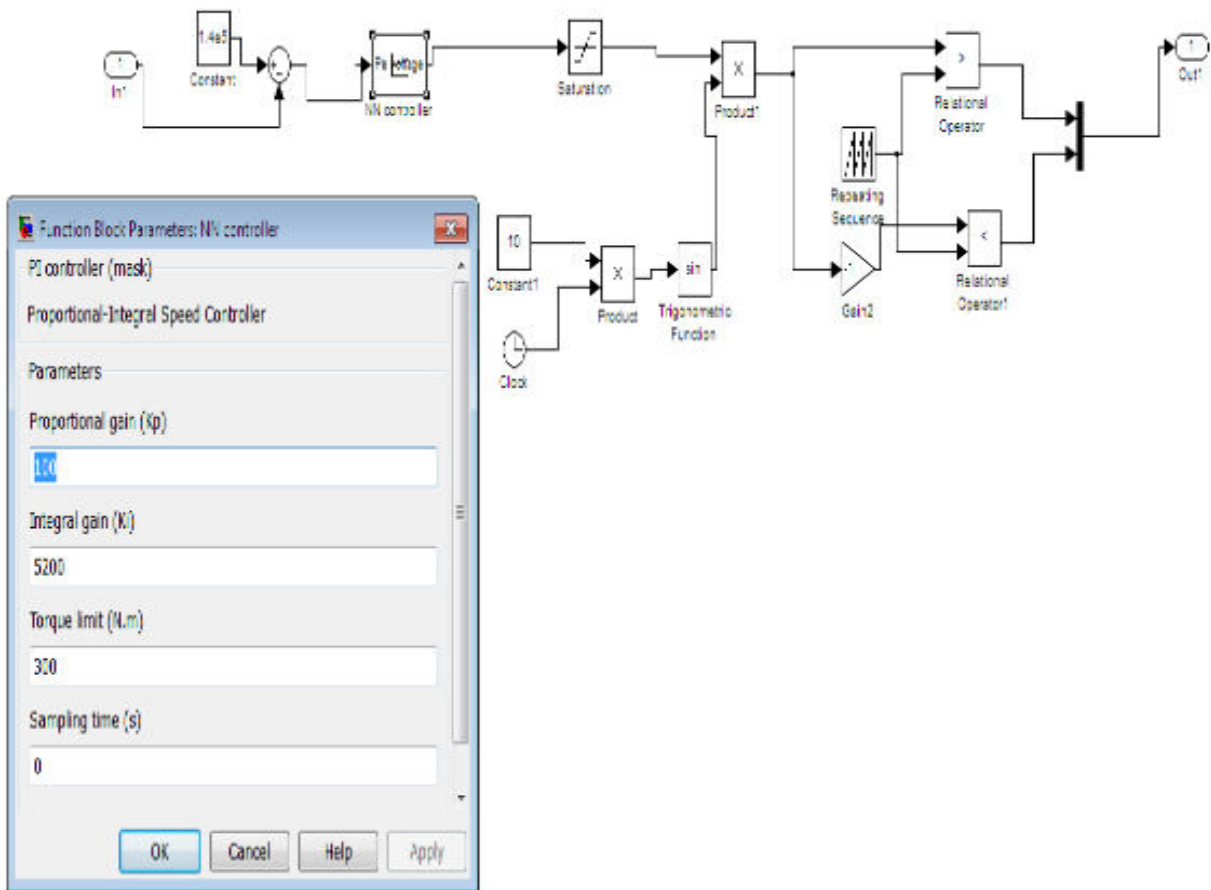


Figure 10: Subsystem of NN controller

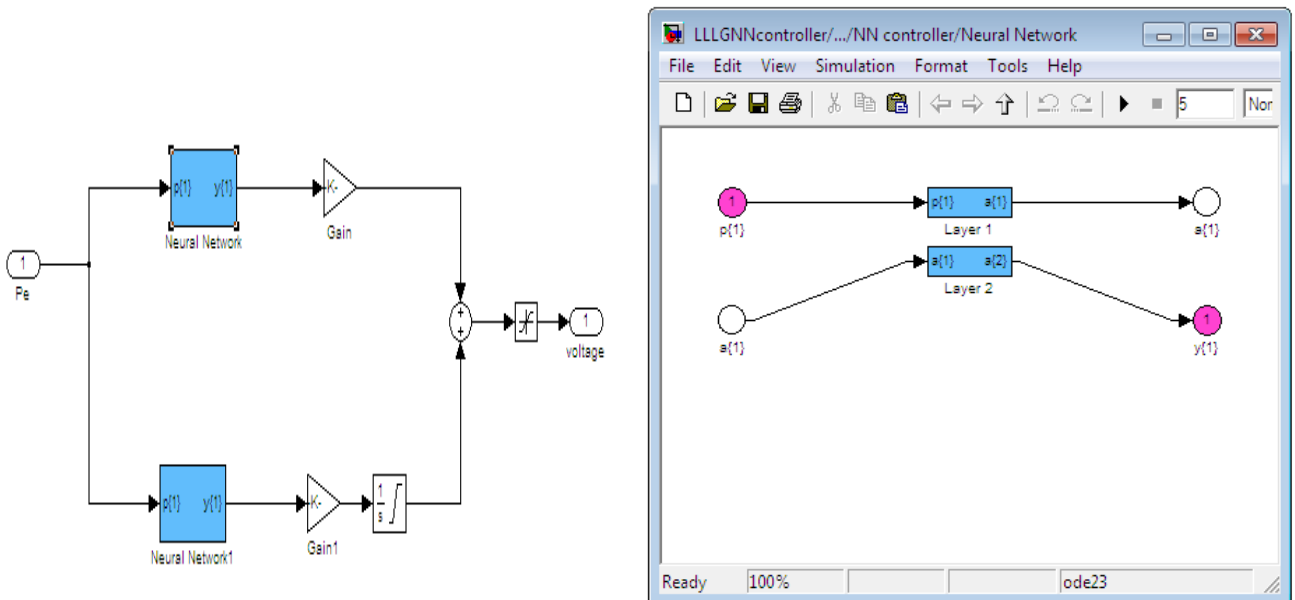


Figure11: Subsystem of NN controller with Hidden Layers

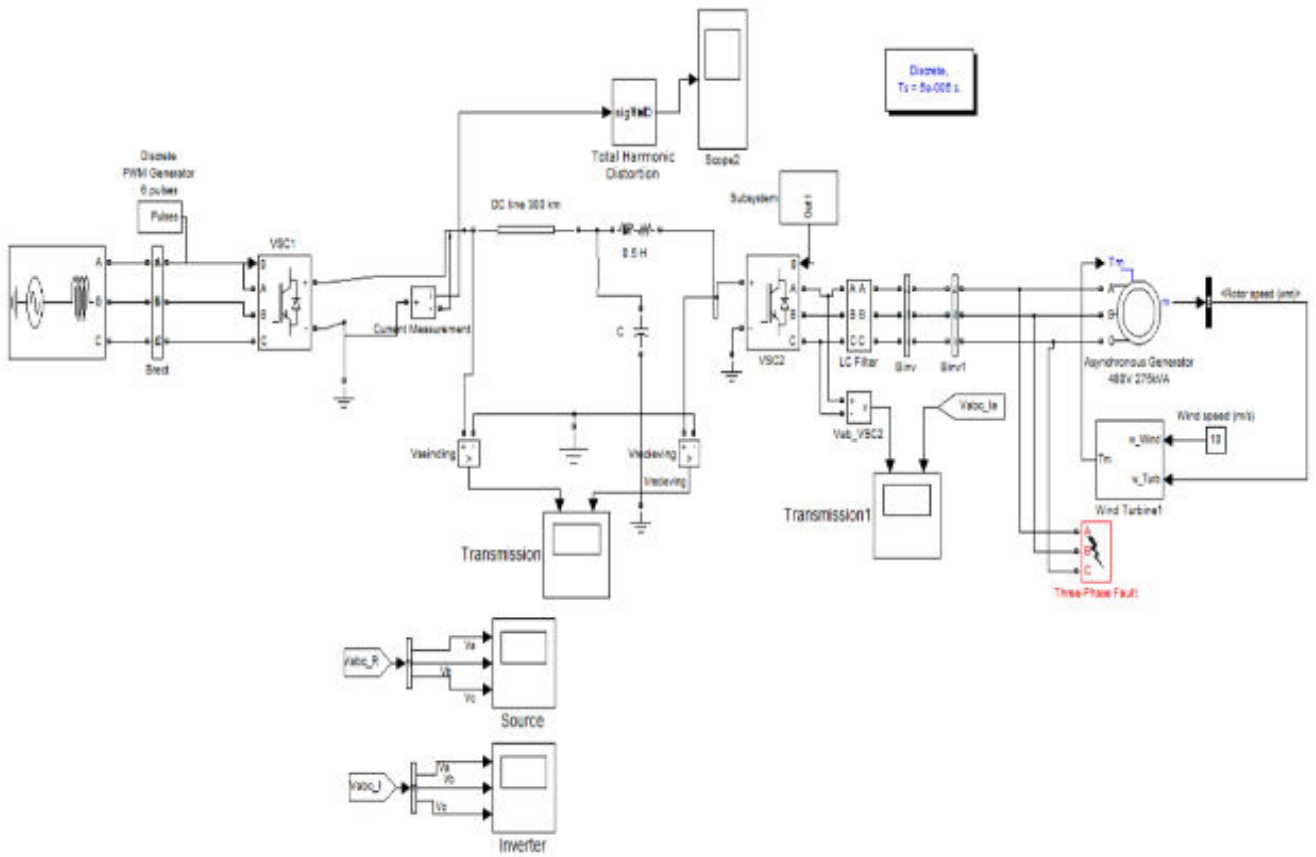


Figure 12: Fault-Error-Suppressing System (FESS)-Free Model of Grid-Connected Variable Speed Control (VSC) HVDC Offshore Wind Farms

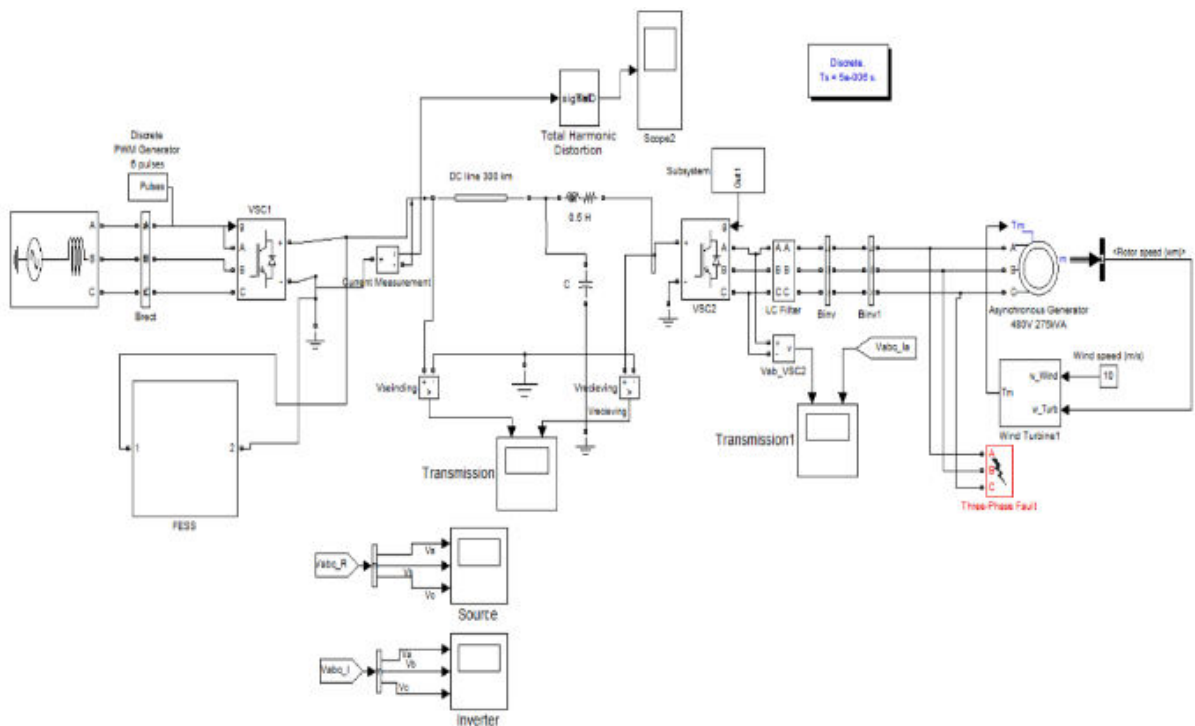


Figure 13: Fault-Error-Susceptibility Evaluation System for Grid-Connected Variable-Speed HVDC Offshore Wind Farms

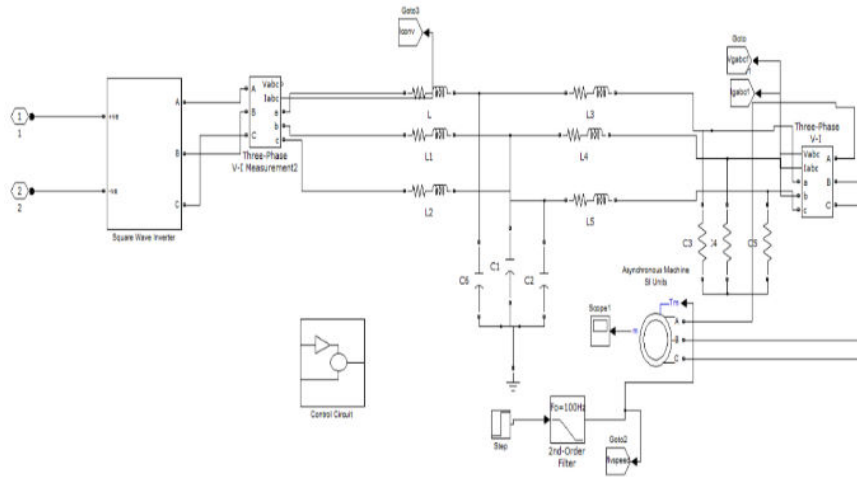


Figure 14: Flywheel Energy Storage System Subsystem

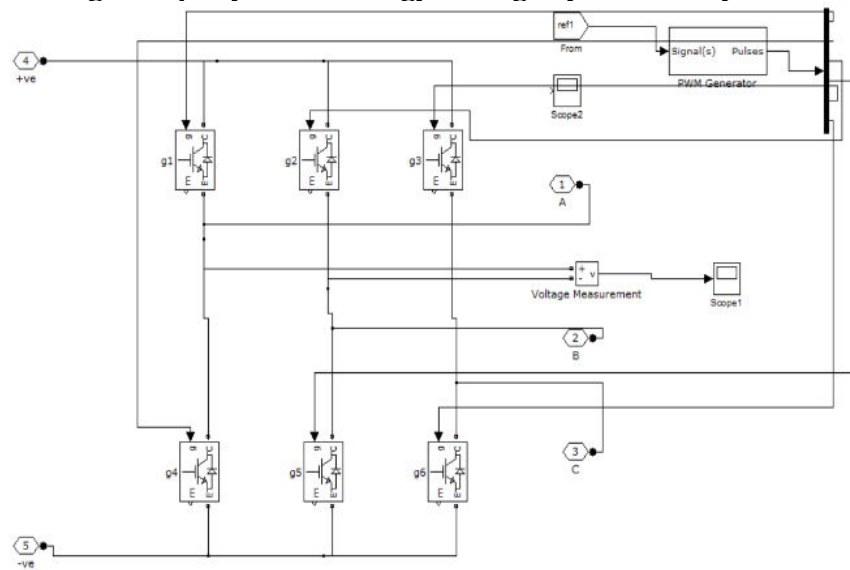


Figure 15: Subsystem of Square wave Inverter

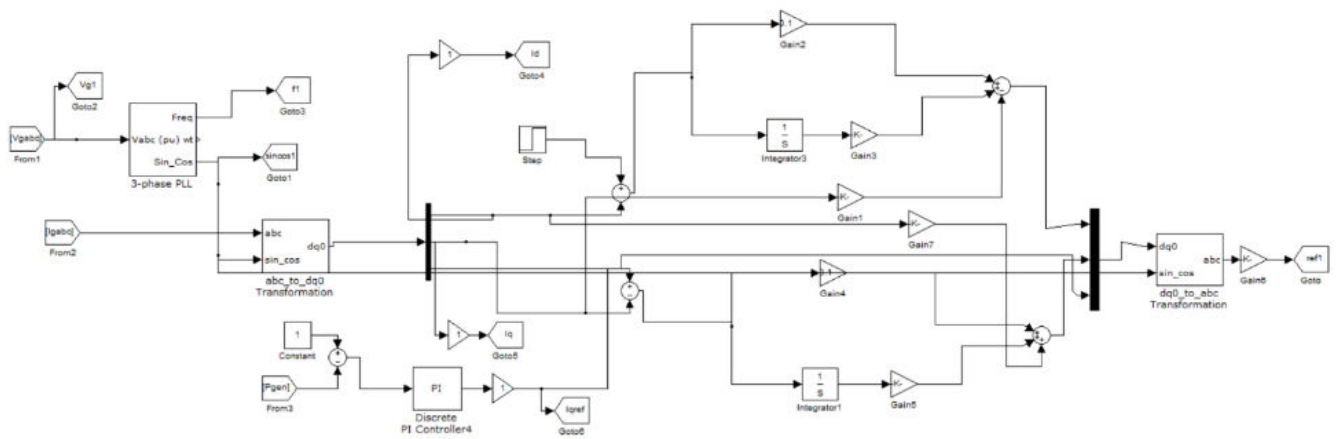


Figure16: Sub system of control circuit

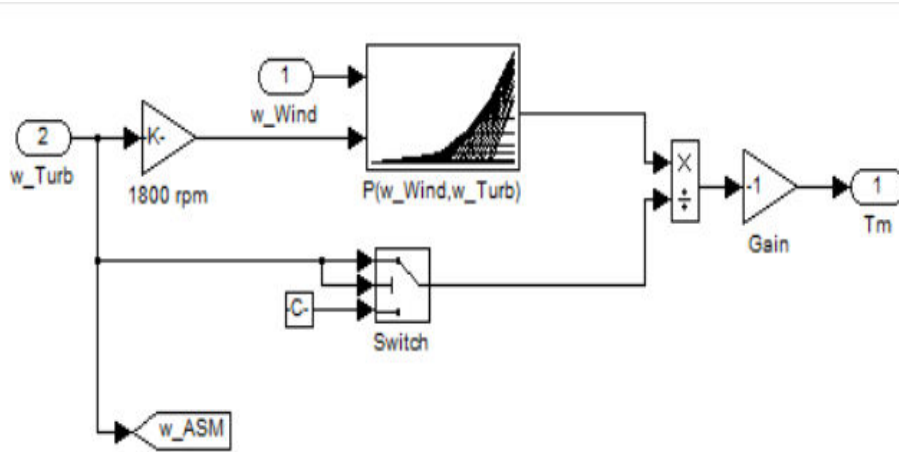


Figure17: Subsystem of Wind Turbine characteristics

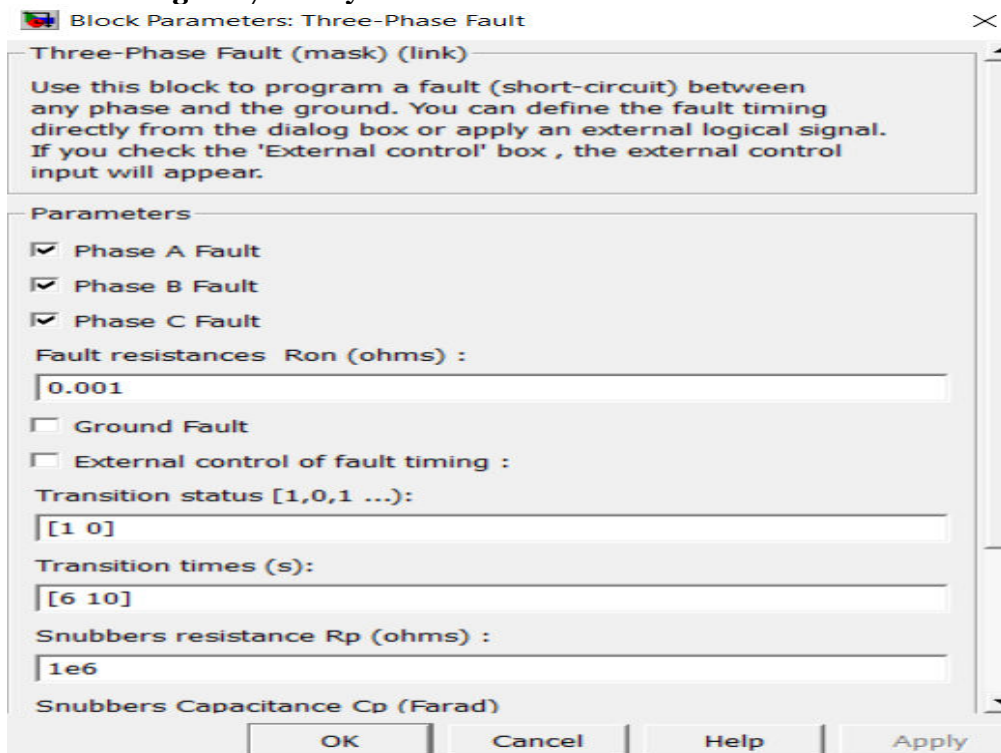


Figure18: Three - Phase Fault Block parameters

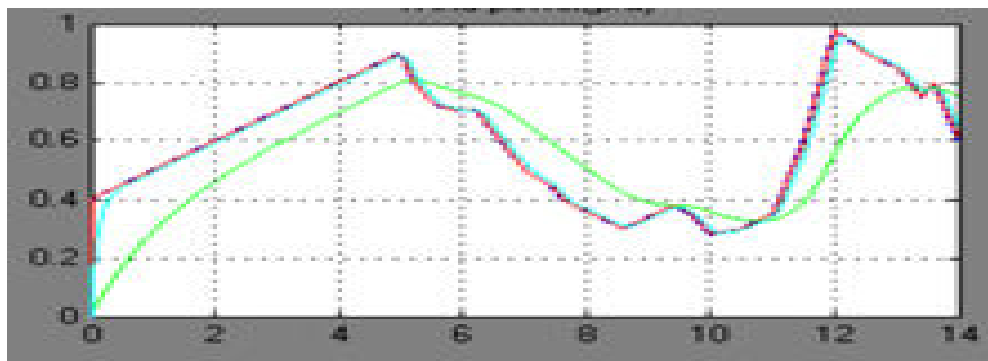


Figure19: Wind power Versus time (secs) with PID, NN controllers

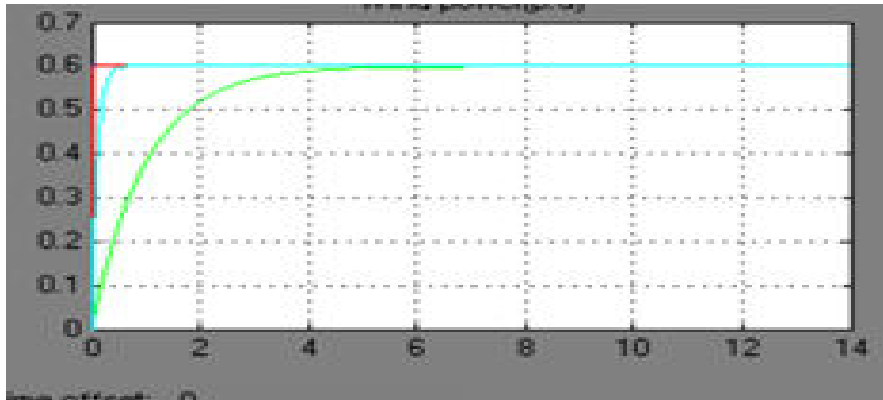


Figure20: Grid power Versus time (secs) with PID, NN controllers

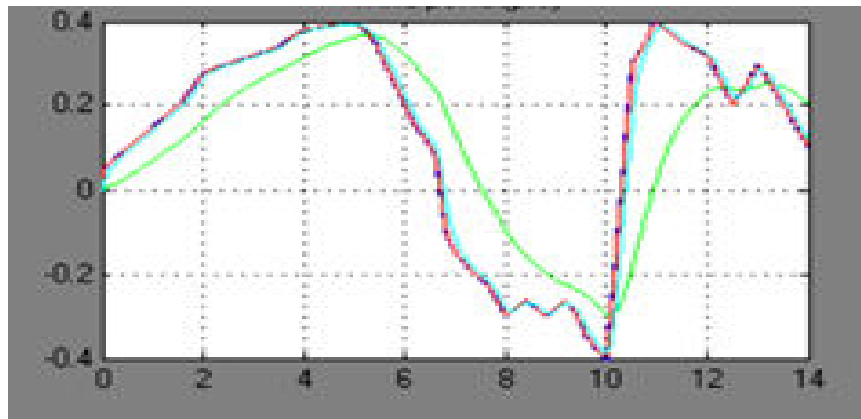


Figure 21: Free-wheeling power Versus time (secs) with PID, NN controllers

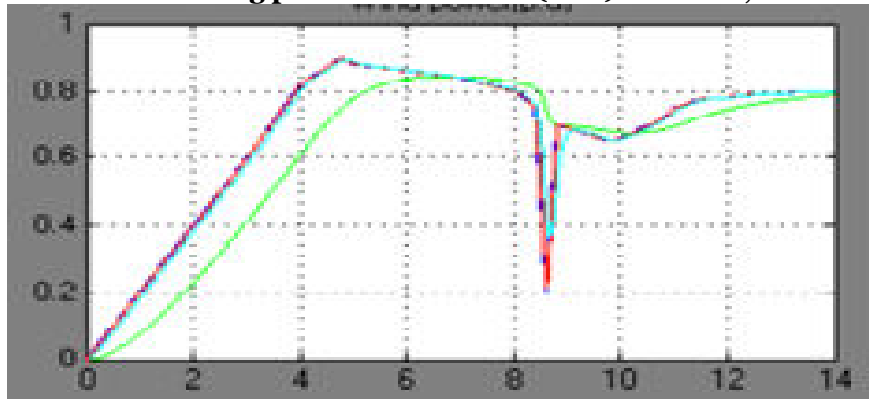


Figure22: Free-wheeling speed Versus time (secs) with PID, NN controllers

Table 2: Comparison of Simulation results without and with FESS

S.No		Wind power (P.u)		Grid power (P.u)		Inverter Voltage (P.u)		Inverter current (P.u)	
		%M _p	t _s (secs)	%M _p	t _s (secs)	%M _p	t _s (secs)	%M _p	t _s (secs)
1	Without FESS	0.062	0.52	0.0485	0.35	0.032	0.41	0.041	0.36
2	With FESS	0.052	0.18	0.0396	0.14	0.0283	0.28	0.041	0.21

Table 3: Comparison of Simulation results with FESS for different faults

S.No	Faults	Wind power (P.u)		Grid power (P.u)		Freewheeling Power (P.u)		Freewheeling speed (P.u)	
		%M _p	t _s (secs)	%M _p	t _s (secs)	%M _p	t _s (secs)	%M _p	t _s (secs)
1	No	0.0521	0.18	0.0396	0.14	0.0621	0.21	0.0561	0.32
2	LG	0.053	0.23	0.041	0.3	0.058	0.2	0.058	0.38
3	LLG	0.056	0.28	0.0425	0.38	0.051	0.42	0.0601	0.45
4	LLLG	0.062	0.33	0.049	0.42	0.061	0.47	0.062	0.66
5	LLL	0.0601	0.45	0.052	0.49	0.058	0.32	0.0485	0.38

Analysis: The case study simulates the system's operation both before and after the addition of the FESS to the network, comparing the two sets of data. An FESS rating is determined by comparing the usual operation of power levelling, in which energy is charged or discharged for a longer duration than in a fault scenario, to the actual operation. We assume that the FESS latency consistent H is 5 s. While the proposed framework request is 0.6 pu, the wind power ranges from 1 pu to 0.2 pu. Tables 2 and 3 show that in the worst-case scenario, the FESS is expected to be able to sustain 40% of the total wind farm rating.

Table 4: Comparison of THD for faults applied at Grid side

S.No	Faults	Grid current THD
1	LG	0.01
2	LLG	0.2612
3	LLLG	0.2617
4	LLL	0.2613

Analysis: The total harmonic distortion at grid-side connected faults are estimated by using FFT analysis. From Table 4, it is observed that LLLG fault have high THD than compared to other faults.

Table 5: Comparison of Simulation results with FESS and LLLG fault for different Controllers

S.No	Controllers	Wind power (P.u)		Grid power (P.u)		Freewheeling Power (P.u)		Freewheeling speed (P.u)	
		%M _p	t _s (secs)	%M _p	t _s (secs)	%M _p	t _s (secs)	%M _p	t _s (secs)
1	PID	0.062	0.33	0.049	0.42	0.061	0.47	0.0062	0.66
2	NN	0.012	0.02	0.042	0.29	0.058	0.32	0.047	0.42

Table 6: Comparison of THD for faults applied at Grid side for different controllers

S.No	Controllers	Grid current THD
1	PID	0.612
2	NN	0.261

Analysis: The total harmonic distortion at grid-side connected faults is estimated by using FFT analysis. From Table 5 and 6, it is observed that Neural network been used for reducing THD in wind power, grid power, free-wheeling power and free-wheeling speed versus time (secs).

Conclusion

The purpose of this research is to examine fault ride-through in an HVDC transmission system that is linked to an AC network and operates on electricity generated by offshore wind farms. We have covered many faults ride-through methods. We provide a novel FESS-based control method that makes use of the DC link voltage controller to release energy in the FESS from the DC link. To get the most out of the linked storage system, the suggested FESS is also used for power levelling when the system is running normally. Two distinct control narratives are used in the applied control method, one for each fault condition indicated by the DC link voltage level. The suggested FESS design offers quick reaction and reliable performance for fault ride-through and power levelling, according to the findings of both simulations and experiments. By making use of the trapped energy during a fault, the suggested FESS simulation model outperforms the various fault ride-through strategies which have been addressed. Also, the offshore wind farm station will not be interrupted, which guarantees the total system's sustainability. The suggested system has few moving parts and little maintenance needs, but it has a high converter rating and a high starting price, which are two big negatives.

References

1. Kezunovic M, Rikalo I, Sobajic DJ, "Real-time and Off-line Transmission Line Fault Classification Using Neural Networks", *Engineering Intelligent Systems*, vol. 10, 1996, pp. 57-63.
2. L. Harnefors, "Design and analysis of general rotor-flux-oriented vector control systems," *IEEE Trans. Ind. Electron.*, vol. 48, no. 2, pp. 383-390, Apr. 2001
3. Cárdenas, R.; Pena, R.; Asher, G.; Clare, J. Control strategies for enhanced power smoothing in wind energysystems using a flywheel driven by a vector-controlled induction machine. *IEEE Trans. Ind. Electron.* 2001, 48, 625-635.
4. S. Hahn, W. Kim, J. Kim, C. Koh, and S. Hahn, "Low speed FES with induction motor and generator," *IEEE Trans. Appl. Supercond.*, vol. 12, no. 1, pp. 746-749, Mar. 2002.
5. S. Samineni, B. K Johnson, H. L Hess, and J. D. Law, "Modeling and analysis of a flywheel energy storage system with a power converter interface," in *Proc. Int. Conf. Power Systems Transients-IPST 2003*, New Orleans, LA, USA.
6. J. Zhang, "Research on Flywheel Energy Storage System Using in Power Network," in *Proc. Int. Conf. Power Electronics and Drives Systems, PEDS*, Nov. 28-01, 2005, vol. 2, pp. 1344-1347.
7. S. Samineni, B. K. Johnson, H. L. Hess, and J. D. Law, "Modeling and analysis of a flywheel energy storage system for Voltage sag correction," *IEEE Trans. Ind. Application.*, vol. 42, no. 1, pp. 42-52, Jan.-Feb. 2006.
8. Y. M. Meng, T. C. Li, and L. Wang, "Simulation of controlling methods to flywheel energy storage on charge section," in *Proc. 3rd Int. Conf. Electric Utility Deregulation and Restructuring and Power Technologies, DRPT*, Apr. 6-9, 2008, pp. 2598-2602.
9. N. Flourentzou, V. G. Agelidis, and G. D. Demetriades, "VSC-Based HVDC power transmission systems: An overview," *IEEE Trans. Power Electron.*, vol. 24, no. 3, pp. 592-602, Mar. 2009.
10. C. Feltes, H. Wrede, F. W. Koch, and I. Erlich, "Enhanced fault ridethrough method for wind farms connected to the grid through VSCbased HVDC transmission," *IEEE Trans. Power Syst.*, vol. 24, no. 3, pp. 1537-1546, Aug. 2009.
11. L. Rennian and W. Xin, "Status and challenges for offshore wind energy," in *Proc. Int. Conf. Materials for Renewable Energy & Environment (ICMREE)*, May 20-22, 2011, pp. 601-605.
12. Arani, A.K.; Karami, H.; Gharehpetian, G.; Hejazi, M. Review of Flywheel Energy Storage Systems structures and applications in power systems and microgrids. *Renew. Sustain. Energy Rev.* 2017, 69, 9-18.
13. Soomro, A.; Amiryar, M.E.; Pullen, K.R.; Nankoo, D. Comparison of performance and controlling schemes of synchronous and induction machines used in flywheel enregy storage systems. *Energy Procedia* 2018, 151, 100-110.